GEOLOGY | THE GEOLOGICAL SOCIETY OF AMERICA®

https://doi.org/10.1130/G54000.1

Manuscript received 22 September 2025
Revised manuscript received 22 November 2025
Manuscript accepted 5 December 2025

Published online 24 December 2025

Melting the myth: Prograde garnet dissolves during early crustal melting

Lucas R. Tesser[1,2,*], Pierre Lanari[2], Jacob B. Forshaw[3], Thorsten A. Markmann[4], Mathias Hueck[5], Benita Putlitz[2], Noralinde de Leijer[2], Cauê R. Cioffi[1], Miguel A.S. Basei[1], and Carlos E. Ganade[6]

[1]Institute of Geosciences, University of São Paulo, São Paulo 05508-080, Brazil
[2]Institute of Earth Sciences, University of Lausanne, Lausanne, Switzerland CH-1015
[3]Mineral Deposit Research Unit, Vancouver, British Columbia V6 T 1Z4, Canada
[4]Institute of Geological Sciences, University of Bern, Bern CH-3012, Switzerland
[5]Institute of Geosciences, Ruhr-University Bochum, Bochum 44801, Germany
[6]Centre of Applied Geosciences, Brazilian Geological Survey, Rio de Janeiro 22290-255, Brazil

ABSTRACT

Garnet is widely thought to increase in stability and volume during prograde metamorphism and partial melting. Yet, whether early-formed subsolidus garnet persists or breaks down when melting begins remains an open question. Here, we integrate 3-D X-ray tomography with high-resolution major- and trace-element mapping of centrally sectioned garnets across a metapelitic metamorphic sequence to track their response from the subsolidus-suprasolidus transition to melting temperatures up to ~770 °C. Contrary to experimental and phase equilibrium predictions, garnet undergoes extensive dissolution at the onset of partial melting, losing >40% of its volume. Melt percolation creates internal cavity networks within garnet, connecting crystal interiors to the reactive matrix, markedly shortening intracrystalline diffusion pathways at the melt-crystal interface. This process leads to the consumption of garnet and results in major- and trace-element redistribution at temperatures too low for intracrystalline diffusion in larger grains. Our findings reconcile the long-standing discrepancy between predicted progressive garnet growth above the solidus and the scarcity of melt inclusions in garnet rims in migmatites and granulites. As partial melting begins, subsolidus garnet reacts and becomes a permeable heavy rare earth elements and yttrium (HREE-Y) reservoir in the residual crust.

INTRODUCTION

Garnet is a cornerstone mineral for interpreting deep crustal processes and exerts a first-order control on the availability of heavy rare earth elements and yttrium (HREE-Y) during partial melting. This hinges on the key assumption, derived from melting experiments and phase equilibrium models, that garnet remains inert or may even increase in abundance above the solidus (Patiño Douce and Johnston, 1991; Patiño Douce and Harris, 1998; Vielzeuf and Schmidt, 2001; Baxter et al., 2017). In metasedimentary rocks, fluid-absent muscovite dehydration melting initiates at ~650–750 °C via the reaction muscovite + plagioclase + quartz = aluminosilicate + K-feldspar + melt, producing peraluminous melts without involving garnet. Melting progresses via incongruent biotite breakdown at ~750–850 °C via the reaction biotite + aluminosilicate + plagioclase + quartz = garnet + K-feldspar + melt, generating metaluminous melts with garnet and K-feldspar as peritectic phases, thereby reinforcing the paradigm that garnet abundance and stability progressively increase above the solidus.

Nevertheless, the natural rock record suggests a more complicated story. Garnet-hosted melt inclusions occur mainly in the cores of peritectic garnets, implying that pre-existing subsolidus crystals were recrystallized or lost before new growth (e.g., Carvalho et al., 2025). Garnet instability during high-grade metamorphism has been invoked to explain Lu-Hf isotopic disequilibrium signatures in granulites (Moreira et al., 2023) and mismatches between residual rocks and their extracted melts (e.g., Xia et al., 2022; Yang et al., 2022). At the grain scale, HREE-Y signatures in granulite-facies garnets reflect late peritectic regrowth or interface-coupled dissolution-precipitation replacement (Ague and Axler, 2016; Rubatto et al., 2020; Goncalves et al., 2021; Smit et al., 2024).

Our approach builds on two fundamental principles applied to a progressive metamorphic sequence from the Sergipano belt, northeastern Brazil. Firstly, because higher-grade rocks have passed through similar pressure-temperature (*P-T*) conditions as their low-grade equivalents, the sequence provides a natural framework for tracing the evolution of subsolidus garnets during partial melting. Secondly, the largest garnet porphyroblasts typically nucleate earlier and thus retain the most complete petrological record (George and Gaidies, 2017). Based on these ideas, we integrate 3-D garnet distributions with high-resolution chemical mapping of the largest, centrally sectioned garnet crystals across the sequence to evaluate how subsolidus garnet responds to early crustal melting.

GEOLOGICAL SETTINGS AND SAMPLING STRATEGY

The Sergipano belt in northeastern Brazil provides an exceptional natural laboratory to investigate garnet behavior across the solidus. Its eastern segment exposes a metamorphic sequence formed during the late Neoproterozoic collision between the São Francisco craton and the Pernambuco-Alagoas block (Oliveira et al., 2010). Six metamorphic zones defined by index mineral assemblages in metapelites were mapped: biotite, garnet, staurolite-kya-

Lucas R. Tesser https://orcid.org/0000-0001-7253-7630
*ltesser.geo@gmail.com

CITATION: Tesser, L.R., et al., 2026, Melting the myth: Prograde garnet dissolves during early crustal melting: Geology, v. XX, p. , https://doi.org/10.1130/G54000.1

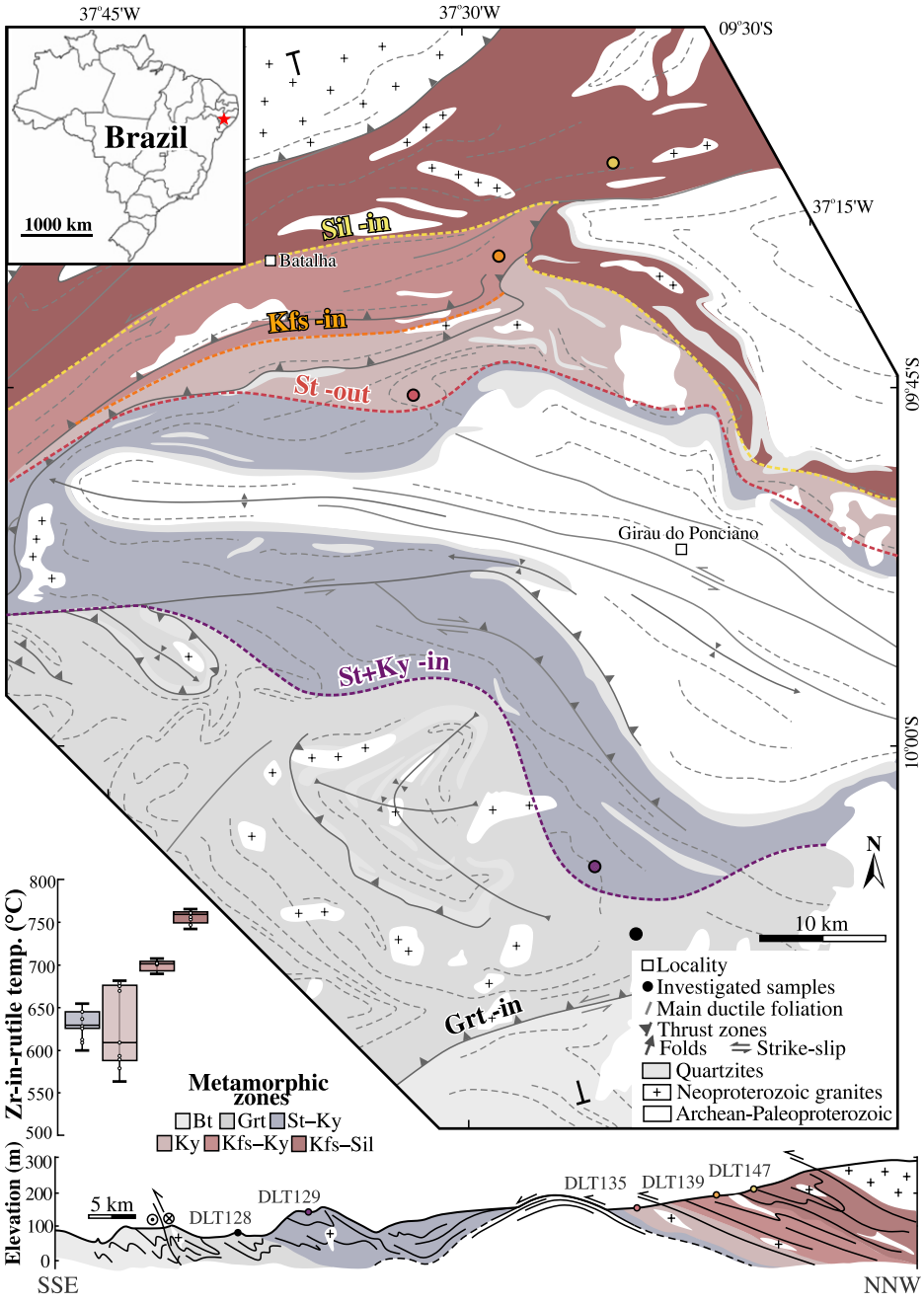

Figure 1. Simplified metamorphic map and cross section of eastern Sergipano belt in northeastern Brazil showing distribution of metamorphic zones, isograds, main ductile structures, and plutons. Dots in map represent location of studied samples. Lower-left panel depicts distribution of Zr-in-rutile temperatures across the sequence. Bt—biotite; Grt—garnet; St—staurolite; Ky—kyanite; Kfs—K-feldspar; Sil—sillimanite.

nite, kyanite, K-feldspar–kyanite, and K-feldspar–sillimanite (Fig. 1). The first appearance of K-feldspar prior to sillimanite marks the initiation of muscovite-dehydration melting and characterizes the high-pressure mineral assemblage sequence (Pattison and Forshaw, 2025). Zr-in-rutile content increases across the sequence, yielding maximum temperatures of ~770 °C (Fig. 1).

To track garnet evolution, we selected compositionally comparable garnet-bearing metapelites from each zone. Cylindrical cores were drilled from hand samples and scanned using microcomputed tomography (μCT), providing high-resolution 3-D images of garnet distributions. In each sample, the largest garnet crystal was selected and cut through its equatorial section. The resulting rock slices were mounted and polished to expose the geometric center of the crystals for analysis. High-resolution elemental maps were acquired using electron probe microanalysis (EPMA) and laser ablation–inductively coupled plasma–mass spectrometry (LA-ICP-MS). Further analytical details, sample locations, and geochemistry are provided in the Supplemental Material[1].

TRACKING GARNET DISTRIBUTION ACROSS THE SOLIDUS

Petrographic observations reveal systematic changes in garnet texture and inclusion assemblages across the solidus. Subsolidus garnets (garnet to kyanite zones) exhibit sharp grain boundaries and host inclusions of prograde minerals such as quartz, muscovite, biotite, staurolite, ilmenite, and rutile (Figs. 2A–2C). In contrast, suprasolidus garnets (K-feldspar–kyanite and K-feldspar–sillimanite zones) display deeply embayed boundaries and host polycrystalline quartzofeldspathic domains (Figs. 2D and 2E) interpreted as former melt pockets. Rather than being isolated, these pockets form 3-D, channel-like networks connecting the crystal interior to the external matrix (Movie S1 in the Supplemental Material).

This textural shift coincides with a pronounced reduction in garnet modal abundance, from 5.3 ± 0.2, 6.3 ± 0.1, and 5.4 ± 0.1 vol% in three subsolidus samples to 3.5 ± 0.2 and 1.2 ± 0.4 vol% in the two suprasolidus samples (Fig. 2F), representing a net loss of ~42% across the solidus. The number of crystals also declines markedly, from hundreds in subsolidus samples to 117 and 81 in comparably sized suprasolidus samples, ruling out simple volumetric dilution (Table S2 in the Supplemental Material). Crystal size distribution (CSD) analysis reinforces this trend (Fig. 2G). Samples from the garnet and staurolite-kyanite zones show right-skewed CSDs with long tails of large crystals, consistent with protracted growth and nucleation during prograde metamorphism (George and Gaidies, 2017). The kyanite zone sample exhibits a flatter CSD, potentially reflecting grain-size maturation during staurolite breakdown (Chinner, 1961), longer heating time scales, or kinetic suppression of renewed nucleation (Kretz, 1966; Kelly et al., 2013). Suprasolidus CSDs are similarly flat, comparable to that of the kyanite zone sample, and exhibit maximum crystal radii of up to 0.20 mm.

Phase equilibrium simulations of garnet growth along the metamorphic field gradient indicate a limited influence of bulk-rock variability on the garnet volume (Fig. 2H). Models predict the observed subsolidus garnet volume but overestimate the suprasolidus volume by >10%, suggesting a minimal effect of bulk-rock composition on garnet volume loss. Additional

[1]Supplemental Material. Detailed methods and extended results, including Figures S1–S7, Supplemental Tables S1–S4, and Movie S1. Please visit https://doi.org/10.1130/GEOL.S.30811355 to access the supplemental material; contact editing@geosociety.org with any questions.

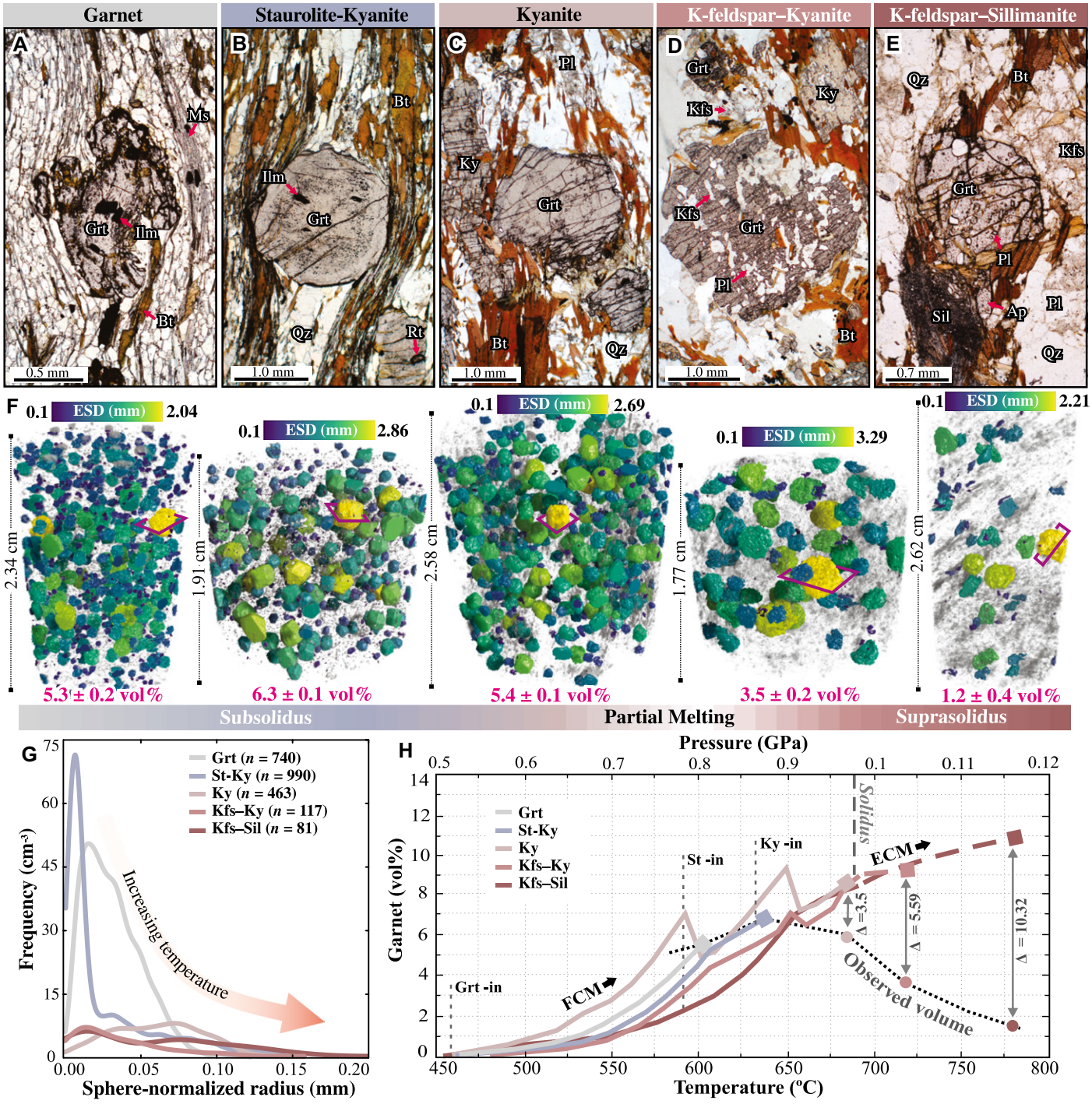

Figure 2. (A–E) Petrographic features of representative garnet grains from garnet (A), staurolite-kyanite (B), kyanite (C), K-feldspar–kyanite (D), and K-feldspar–sillimanite (E) zones. (F) X-ray microcomputed tomography (μCT) reconstructions depicting garnet reduction across the solidus; reconstructions are plotted in scale, and garnet crystals are colored according to individual equivalent spherical diameter (ESD). Total volume of garnet, along with its respective uncertainty, is shown below each sample. Purple squares in largest garnet crystals indicate approximate position where central sections were obtained. (G) Kernel density curves of crystal size distributions showing shift of garnet population distributions with increasing metamorphic grade. (H) Phase equilibrium modeling of prograde garnet growth using whole-rock compositions. The fractional crystallization model (FCM) was applied to subsolidus conditions, and the equilibrium crystallization model (ECM) was used to simulate suprasolidus garnet growth (e.g., Lanari and Engi, 2017). The model systematically overestimates the volume of suprasolidus garnet (Δ = difference in vol%), suggesting the loss of garnet above the solidus cannot be explained by bulk-rock effects alone. Ap—apatite; Bt—biotite; Grt—garnet; Ilm—ilmenite; Kfs—K-feldspar; Ky—kyanite; Ms—muscovite; Pl—plagioclase; Qz—quartz; Rt—rutile; Sil—sillimanite; St—staurolite.

μCT scans from multiple hand specimens across different outcrops consistently reproduced garnet distributions and CSD shifts (Supplemental Material), which suggests that partial melting caused the loss of garnet volume.

ELEMENT (RE)DISTRIBUTION IN METAMORPHIC GARNETS

Garnet is the primary reservoir for HREE-Y in high-grade metamorphic rocks, but the integrity of its geochemical record above the solidus is uncertain. In subsolidus samples, garnet preserves prograde growth zoning consistent with Rayleigh fractionation for major elements (Figs. 3A–3C); however, trace elements reveal a more complex history. The garnet zone

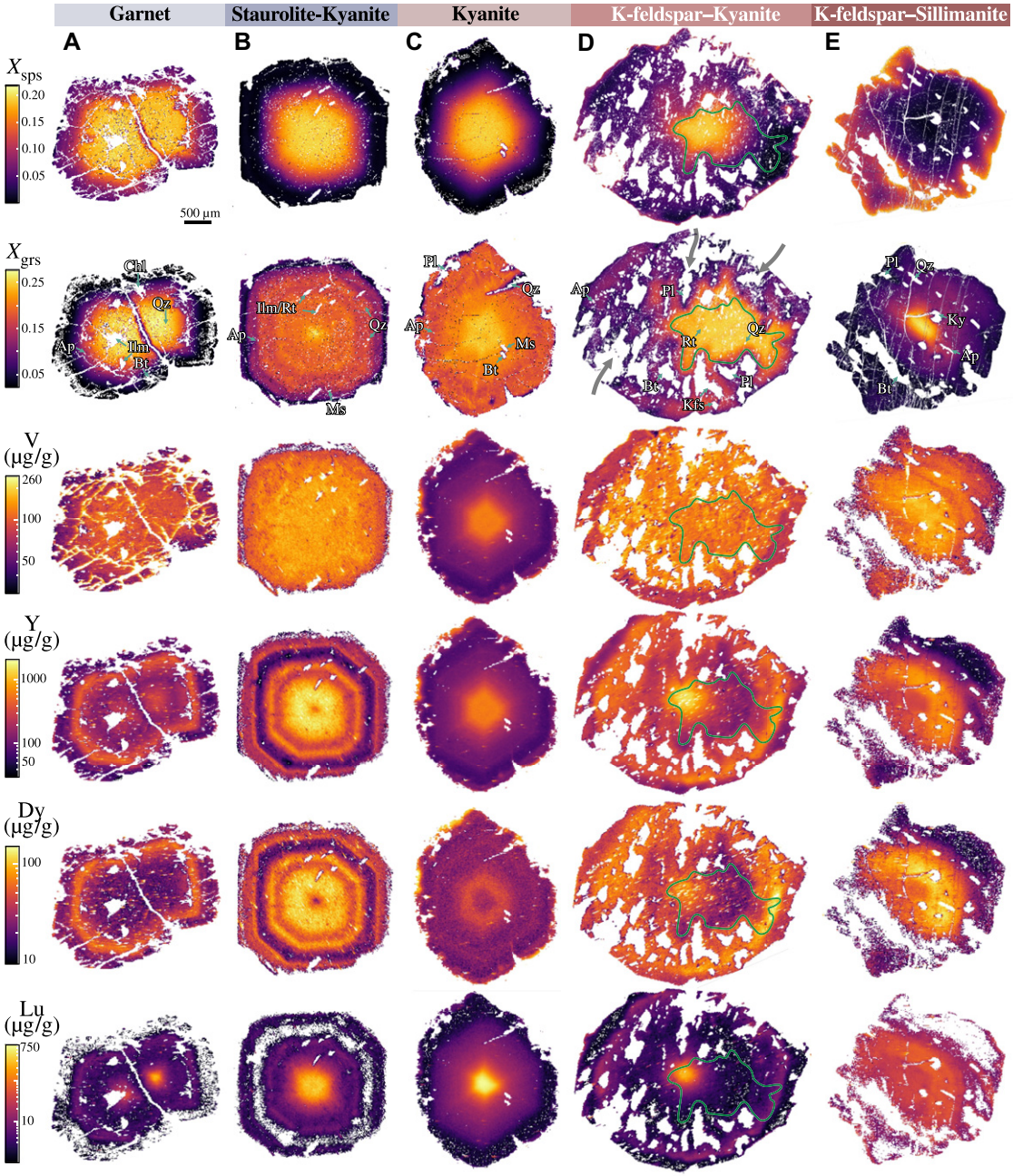

Figure 3. Selected major- and trace-element maps of centrally sectioned garnets from subsolidus (A–C) to suprasolidus (D–E) samples, all using consistent color and size scales for comparison. The calculated end-member maps of spessartine (X_{sps}) and grossular (X_{grs}) show major-element zoning. Vanadium (V), yttrium (Y), dysprosium (Dy), and lutetium (Lu) are displayed on a logarithmic scale. In D, green polygon marks area least affected by melt infiltration, while gray arrows indicate melt-related dissolution features. Maps were calibrated with XMapTools (Lanari et al., 2014; Markmann et al., 2024). Mineral abbreviations: Ap—apatite; Bt—biotite; Chl—chlorite; Ilm—ilmenite; Kfs—K-feldspar; Ky—kyanite; Ms—muscovite; Pl—plagioclase; Qz—quartz; Rt—rutile; St—staurolite.

sample exhibits two HREE-Y–enriched cores surrounded by an annulus, suggesting coalescence of multiple nuclei (Spiess et al., 2001). Staurolite-kyanite zone garnet shows concentric oscillatory HREE-Y zoning, indicating fluctuating trace element supply from matrix mineral reactions (Konrad-Schmolke et al., 2008). Kyanite zone garnet displays bell-shaped HREE-Y and Mn zoning, characteristic of near-equilibrium growth from a homogenized matrix (Yogi et al., 2025).

Suprasolidus garnets, in contrast, exhibit clear evidence of prograde HREE-Y zoning overprint and smoothing by melt-mediated processes. In the K-feldspar–kyanite zone, garnet preserves a concentric HREE-Y spike, interpreted as the remnant subsolidus core (Fig. 3D). This is surrounded by a broad depleted mantle, an enriched annulus, and a final depleted outermost rim. Crystallized melt pockets connected to the external matrix occur mainly outside the limit of the high-Ca core, marking the extent of melt percolation (green polygon in Fig. 3D). These features are inconsistent with any fractional crystallization or intracrystalline-diffusion mechanism alone. Instead, we attribute them to melt-assisted dissolution, which creates interconnected porosity that drastically shortens diffusion pathways along the crystal-melt interface (e.g., Dominguez et al., 2025). This facilitates the rapid outward flux of elements from the dissolving crystal, generating the depleted mantle. Afterward, back-diffusion (Carlson, 2012) or interface-coupled dissolution-precipitation (Putnis, 2009; Ague and Axler, 2016; Goncalves et al., 2021) concentrates these liberated elements into the secondary HREE-Y–rich outer annulus (Fig. 3D). Furthermore, complete dissolution of smaller crystals may also contribute to this enrichment. Co-enrichments of V, Cr, and Zr at the outer annulus suggest contributions from concurrent muscovite and zircon consumption during garnet dissolution. The outermost Zr-depleted rim likely represents final garnet overgrowth from a melt that became undersaturated in HREE-Y due to dilution effects or to concurrent prograde zircon overgrowth (Yakymchuk, 2023).

In the highest-grade K-feldspar–sillimanite zone, evidence for dissolution and enhanced diffusion is more advanced. The original Mn-rich

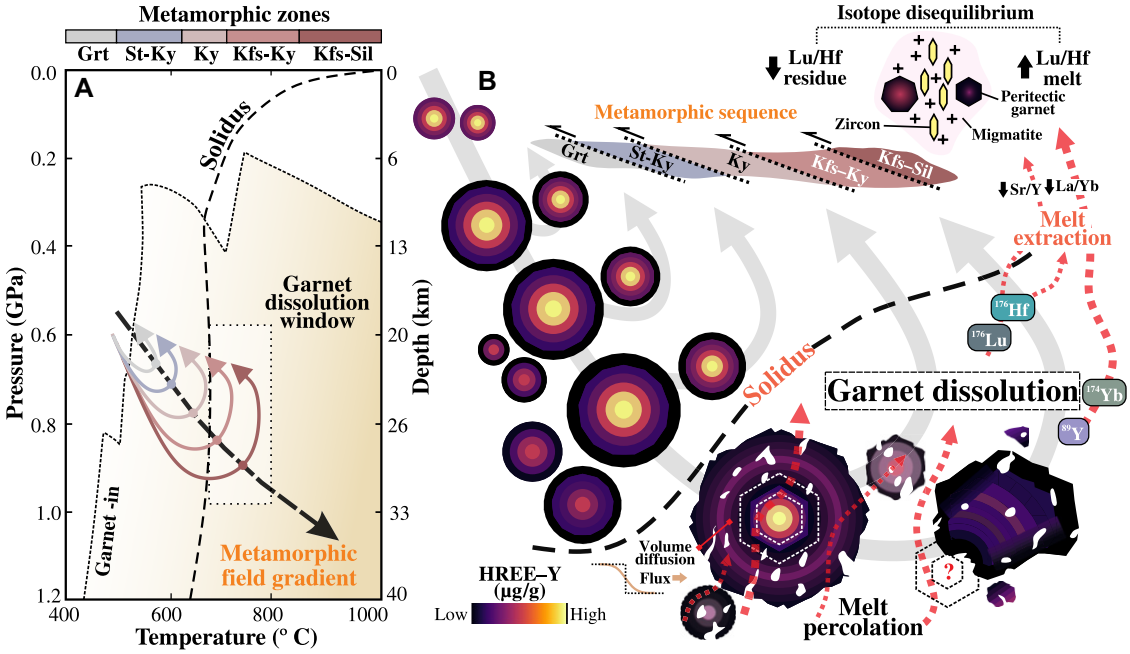

Figure 4. (A) Schematic pressure–temperature paths for five samples spanning from garnet to K-feldspar–sillimanite zones, which reflect increasing metamorphic grade toward the solidus and define a pressure–temperature window in which garnet dissolves. (B) Schematic illustration of how garnet texture, distribution, and heavy rare earth elements and yttrium (HREE-Y) zoning evolve along the metamorphic gradient. Vertical position corresponds to increasing depth/pressure, and the horizontal axis represents increasing temperature toward and beyond the solidus. Subsolidus garnet growth sequesters HREE-Y and retains them until the onset of melting. Above the solidus, melt percolates through the rock and partially dissolves garnet (orange dashed arrows). Melt-assisted dissolution creates an interconnected cavity network linking crystal interiors to the external matrix and enhances re-equilibration via diffusion. As partial melting intensifies, early-formed, HREE-Y-enriched cores are progressively consumed (indicated by the dashed outline and question mark), leaving behind highly modified secondary zoning. Melt extracted near the solidus may carry elevated HREE-Y contents or inherit lutetium/hafnium (Lu/Hf) disequilibrium signatures between the source rock and melt. Synchronous prograde zircon crystallization or later regrowth of peritectic garnet will inherit disturbed melt signatures after significant dissolution of subsolidus garnet. Grt—garnet; St—staurolite; Ky—kyanite; Kfs—K-feldspar; Sil—sillimanite.

core is completely absent, Ca zoning is restricted to a small relict domain, and HREE-Y zoning is reduced to a blurred, curved annulus associated with former melt pockets connected to the matrix (Fig. 3E; Movie S1). This annulus is compositionally and geometrically analogous to the outer annulus observed in the K-feldspar–kyanite zone (Fig. 3D), suggesting an advanced stage of dissolution and loss of the prograde subsolidus core. These findings highlight the efficiency of dissolution as the partial melting intensifies to temperatures of ~770 °C.

GARNET DISSOLUTION EFFECTS ON HREE-Y RETENTION IN THE PARTIALLY MELTED CRUST

Garnet's combination of broad *P-T*-composition stability above the solidus coupled with its ability to retain slow-diffusing elements underpins its importance to petrochronology (Baxter et al., 2017). Our results show, however, that there is a suprasolidus window of ~100 °C in which prograde garnet undergoes extensive melt-assisted dissolution. This adds an additional layer of complexity to petrochronological interpretations: within this interval, melt infiltrates prograde garnet and remobilizes slow-diffusing elements such as Lu and Yb at temperatures far below their conventional closure temperature for large grains (Carlson, 2012; Bloch et al., 2020). Therefore, many zoned granulite-facies garnets may represent extensively modified subsolidus remnants or renewed peritectic growth rather than pristine prograde signatures (e.g., Carvalho et al., 2025). Prograde zoning in migmatitic garnets should therefore be interpreted with caution, particularly when performing thermobarometry. This process also explains why melt inclusions are commonly found in garnet cores rather than in rim overgrowths (Bartoli et al., 2016; Carvalho et al., 2025): subsolidus garnet is removed as partial melting begins, followed by a renewed peritectic nucleation, trapping melt droplets as the garnet volume increases again.

These insights are synthesized in a conceptual model illustrating garnet evolution during progressive metamorphism (Fig. 4). Garnet sequesters HREE-Y during prograde growth but releases part of this budget upon melt-assisted dissolution. While prograde zircon growth may locally retain this flux (Yakymchuk, 2023), continued melt loss means that a portion of the HREE-Y budget is inevitably lost. This has implications for models that interpret high Sr/Y or La/Yb ratios as indicative of high-*P* melting in the garnet-stability field (Chiaradia, 2015; Profeta et al., 2015; Kendrick and Yakymchuk, 2020). Our results suggest that crustal granites may inherit a HREE-Y load from dissolving subsolidus garnet, potentially leading to underestimates of melting depth. Future mass-balance studies are necessary to quantify competition between melt loss and the buffering capacity of zircon and peritectic garnet in retaining HREE-Y in the source. A key outstanding question is whether similar prograde garnet dissolution occurs during partial melting of other protoliths.

Our findings also have implications for the Lu-Hf isotopic budget of continental reservoirs. Remobilization of Lu from subsolidus garnet into extracted melts can shift Lu/Hf ratios to more radiogenic values, particularly if garnet had accumulated significant radiogenic ^{176}Hf prior to dissolution. Although this mechanism has recently been proposed (Gao et al., 2022; Xia et al., 2022; Yang et al., 2022; Moreira et al., 2023), it remains untested. Our study provides new evidence that dissolution of prograde garnet may contribute to the εHf variability commonly observed in crust-derived magmas.

Overall, our results show that garnet cannot be treated as an inert phase during muscovite-dehydration melting of metapelites. Garnet dissolution during early suprasolidus conditions can redistribute trace elements and modify Lu/Hf ratios in crustal magmas, requiring a reassessment of how garnet is incorporated into models of crustal differentiation and melt evolution.

ACKNOWLEDGMENTS

This project has received funding from the Serrapilheira Institute (1709-21887), São Paulo Research Foundation (FAPESP) (2021/06106-1), European Research Council (ERC) under the European Union's Horizon 2020 research innovation program (850530), and Fundação Carlos Chagas Filho de Amparo à Pesquisa do Estado do Rio de Janeiro (FAPERJ) (E-26/200.281/2023-283567). We thank Philip Hartmeier and Hugo Dominguez for fruitful

discussions and Martin Robyr and Thomas Bovay for their assistance with EPMA analysis and sample preparation at University of Lausanne. We gratefully acknowledge Bruna Carvalho, Chris Yakymchuk, and an anonymous reviewer for their valuable and insightful feedback, which greatly enhanced this manuscript. Urs Schaltegger is thanked for his efficient editorial work. **Data availability:** The raw files for the μCT reconstructions and chemical maps are available through Zenodo at https://doi.org/10.5281/zenodo.16863271.

REFERENCES CITED

Ague, J.J., and Axler, J.A., 2016, Interface coupled dissolution-reprecipitation in garnet from subducted granulites and ultrahigh-pressure rocks revealed by phosphorous, sodium, and titanium zonation: American Mineralogist, v. 101, p. 1696–1699, https://doi.org/10.2138/am-2016-5707.

Bartoli, O., Acosta-Vigil, A., Ferrero, S., and Cesare, B., 2016, Granitoid magmas preserved as melt inclusions in high-grade metamorphic rock: American Mineralogist, v. 101, p. 1543–1559, https://doi.org/10.2138/am-2016-5541CCBYNCND.

Baxter, E.F., Caddick, M.J., and Dragovic, B., 2017, Garnet: A rock-forming mineral petrochronometer, *in* Kohn, M.J., et al., eds., Petrochronology: Methods and Applications: Mineralogical Society of America and Geochemical Society Reviews in Mineralogy and Geochemistry 83, p. 469–533, https://doi.org/10.2138/rmg.2017.83.15.

Bloch, E.M., Jollands, M.C., Devoir, A., Bouvier, A.-S., Ibañez-Mejia, M., and Baumgartner, L.P., 2020, Multispecies diffusion of yttrium, rare earth elements and hafnium in garnet: Journal of Petrology, v. 61, https://doi.org/10.1093/petrology/egaa055.

Carlson, W.D., 2012, Rates and mechanism of Y, REE, and Cr diffusion in garnet: American Mineralogist, v. 97, p. 1598–1618, https://doi.org/10.2138/am.2012.4108.

Carvalho, B.B., Bartoli, O., and Cesare, B., 2025, Melt inclusions in high-grade metamorphic rocks: Journal of Petrology, v. 66, https://doi.org/10.1093/petrology/egaf053.

Chiaradia, M., 2015, Crustal thickness control on Sr/Y signatures of recent arc magmas: An Earth scale perspective: Scientific Reports, v. 5, https://doi.org/10.1038/srep08115.

Chinner, G.A., 1961, The origin of sillimanite in Glen Clova, Angus: Journal of Petrology, v. 2, p. 312–323, https://doi.org/10.1093/petrology/2.3.312.

Dominguez, H., Mäder, N., and Lanari, P., 2025, Simulating major element diffusion in garnet using realistic 3D geometries: Computers & Geosciences, v. 206, https://doi.org/10.1016/j.cageo.2025.106023.

Gao, P., Yakymchuk, C., Zhang, J., Yin, C., Qian, J., and Li, Y., 2022, Preferential dissolution of uranium-rich zircon can bias the hafnium isotope compositions of granites: Geology, v. 50, p. 336–340, https://doi.org/10.1130/G49656.1.

George, F.R., and Gaidies, F., 2017, Characterisation of a garnet population from the Sikkim Himalaya: Insights into the rates and mechanisms of porphyroblast crystallisation: Contributions to Mineralogy and Petrology, v. 172, 57, https://doi.org/10.1007/s00410-017-1372-y.

Goncalves, P., Raimondo, T., Paquette, J.-L., and Santos de Souza de Oliveira, J., 2021, Garnet as a monitor for melt–rock interaction: Textural, mineralogical, and compositional evidence of partial melting and melt-driven metasomatism: Journal of Metamorphic Geology, v. 39, p. 617–648, https://doi.org/10.1111/jmg.12592.

Kelly, E.D., Carlson, W.D., and Ketcham, R.A., 2013, Magnitudes of departures from equilibrium during regional metamorphism of porphyroblastic rocks: Journal of Metamorphic Geology, v. 31, p. 981–1002, https://doi.org/10.1111/jmg.12053.

Kendrick, J., and Yakymchuk, C., 2020, Garnet fractionation, progressive melt loss and bulk composition variations in anatectic metabasites: Complications for interpreting the geodynamic significance of TTGs: Geoscience Frontiers, v. 11, p. 745–763, https://doi.org/10.1016/j.gsf.2019.12.001.

Konrad-Schmolke, M., Zack, T., O'Brien, P.J., and Jacob, D.E., 2008, Combined thermodynamic and rare earth element modelling of garnet growth during subduction: Examples from ultrahigh-pressure eclogite of the Western Gneiss Region, Norway: Earth and Planetary Science Letters, v. 272, p. 488–498, https://doi.org/10.1016/j.epsl.2008.05.018.

Kretz, R., 1966, Grain-size distribution for certain metamorphic minerals in relation to nucleation and growth: The Journal of Geology, v. 74, p. 147–173, https://doi.org/10.1086/627152.

Lanari, P., and Engi, M., 2017, Local bulk composition effects on metamorphic mineral assemblages, *in* Kohn, M.J., et al., eds., Petrochronology: Methods and Applications: Mineralogical Society of America and Geochemical Society Reviews in Mineralogy and Geochemistry 83, p. 55–102, https://doi.org/10.2138/rmg.2017.83.3.

Lanari, P., Vidal, O., De Andrade, V., Dubacq, B., Lewin, E., Grosch, E.G., and Schwartz, S., 2014, XMapTools: A MATLAB©-based program for electron microprobe X-ray image processing and geothermobarometry: Computers & Geosciences, v. 62, p. 227–240, https://doi.org/10.1016/j.cageo.2013.08.010.

Markmann, T.A., Lanari, P., Piccoli, F., Pettke, T., Tamblyn, R., Tedeschi, M., Lueder, M., Kunz, B.E., Riel, N., and Laughton, J., 2024, Multiphase quantitative compositional mapping by LA-ICP-MS: Analytical approach and data reduction protocol implemented in XMapTools: Chemical Geology, v. 646, https://doi.org/10.1016/j.chemgeo.2023.121895.

Moreira, H., Dhuime, B., Ionov, D., Buzenchi, A., and Gusev, N., 2023, Hafnium isotope systematics of zircon in high-grade metamorphic rocks of the Anabar shield, Siberia: Radiogenic Hf without mantle input?: Chemical Geology, v. 636, https://doi.org/10.1016/j.chemgeo.2023.121644.

Oliveira, E.P., Windley, B.F., and Araújo, M.N.C., 2010, The Neoproterozoic Sergipano orogenic belt, NE Brazil: A complete plate tectonic cycle in western Gondwana: Precambrian Research, v. 181, p. 64–84, https://doi.org/10.1016/j.precamres.2010.05.014.

Patiño Douce, A.E., and Harris, N., 1998, Experimental constraints on Himalayan anatexis: Journal of Petrology, v. 39, p. 689–710, https://doi.org/10.1093/petroj/39.4.689.

Patiño Douce, A.E., and Johnston, A.D., 1991, Phase equilibria and melt productivity in the pelitic system: Implications for the origin of peraluminous granitoids and aluminous granulites: Contributions to Mineralogy and Petrology, v. 107, p. 202–218, https://doi.org/10.1007/BF00310707.

Pattison, D.R.M., and Forshaw, J.B., 2025, Contact-metamorphosed to regionally-metamorphosed pelites: The natural record: Journal of Petrology, v. 66, https://doi.org/10.1093/petrology/egaf039.

Profeta, L., Ducea, M.N., Chapman, J.B., Paterson, S.R., Gonzales, S.M.H., Kirsch, M., Petrescu, L., and DeCelles, P.G., 2015, Quantifying crustal thickness over time in magmatic arcs: Scientific Reports, v. 5, https://doi.org/10.1038/srep17786.

Putnis, A., 2009, Mineral replacement reactions, *in* Oelkers, E.H., and Schott, J., eds., Thermodynamics and Kinetics of Water-Rock Interaction: Mineralogical Society of America and Geochemical Society Reviews in Mineralogy and Geochemistry 70, p. 87–124, https://doi.org/10.2138/rmg.2009.70.3.

Rubatto, D., Burger, M., Lanari, P., Hattendorf, B., Schwarz, G., Neff, C., Schmidt, P.K., Hermann, J., Vho, A., and Günther, D., 2020, Identification of growth mechanisms in metamorphic garnet by high-resolution trace element mapping with LA-ICP-TOFMS: Contributions to Mineralogy and Petrology, v. 175, 61, https://doi.org/10.1007/s00410-020-01700-5.

Smit, M.A., Vrijmoed, J.C., Scherer, E.E., Mezger, K., Kooijman, E., Schmitt-Kielman, M., Tual, L., Guilmette, C., and Ratschbacher, L., 2024, Retentiveness of rare earth elements in garnet with implications for garnet Lu-Hf chronology: Journal of Metamorphic Geology, v. 42, p. 703–727, https://doi.org/10.1111/jmg.12769.

Spiess, R., Peruzzo, L., Prior, D.J., and Wheeler, J., 2001, Development of garnet porphyroblasts by multiple nucleation, coalescence and boundary misorientation-driven rotations: Journal of Metamorphic Geology, v. 19, p. 269–290, https://doi.org/10.1046/j.1525-1314.2001.00311.x.

Vielzeuf, D., and Schmidt, M.W., 2001, Melting relations in hydrous systems revisited: Application to metapelites, metagreywackes and metabasalts: Contributions to Mineralogy and Petrology, v. 141, p. 251–267, https://doi.org/10.1007/s004100100237.

Xia, Q.-X., Chen, Y.-X., Chen, R.-X., and Zheng, Y.-F., 2022, Elevation of zircon Hf isotope ratios during crustal anatexis: Evidence from migmatites close to the eastern Himalayan syntaxis in southeastern Tibet: Lithos, v. 412–413, https://doi.org/10.1016/j.lithos.2022.106592.

Yakymchuk, C., 2023, Prograde zircon growth in migmatites: Journal of Metamorphic Geology, v. 41, p. 719–743, https://doi.org/10.1111/jmg.12715.

Yang, L., Wang, J.-M., Liu, X.-C., Khanal, G.P., and Wu, F.-Y., 2022, Sr-Nd-Hf isotopic disequilibrium during the partial melting of metasediments: Insight from Himalayan leucosome: Frontiers of Earth Science, v. 10, https://doi.org/10.3389/feart.2022.891960.

Yogi, M.T.A.G., Gaidies, F., Heldwein, O.K.A., and Rice, A.H.N., 2025, The distribution of major and trace elements across a garnet population from the Kalak Nappe Complex (Finnmark, Scandinavian Caledonides): Evidence for size-dependent growth and compositional equilibration in the garnet zone: Journal of Metamorphic Geology, v. 43, p. 613–640, https://doi.org/10.1111/jmg.12820.

Printed in the USA